Permeability retrieval in InP-based waveguide optical device combined with metamaterial

Tomohiro Amemiya,[1,*] Seiji Myoga,[2] Takahiko Shindo,[2] Eijun Murai,[2] Nobuhiko Nishiyama,[2] and Shigehisa Arai[1,2]

[1]*Quantum Nanoelectronics Research Center, Tokyo Institute of Technology, Tokyo 152-8552, Japan*

[2]*Department of Electrical and Electronic Engineering, Tokyo Institute of Technology, Tokyo 152-8552, Japan*

**Corresponding author: amemiya.t.ab@m.titech.ac.jp*

Received February 24, 2012; revised April 2, 2012; accepted April 6, 2012; posted April 9, 2012 (Doc. ID 163670); published June 8, 2012

An InP-based Mach—Zehnder interferometer combined with a metamaterial layer consisting of a split-ring resonator array was constructed to measure the complex permeability of the metamaterial. At a wavelength of 1.5 μm, the metamaterial showed non-unity relative permeability induced by magnetic interaction with propagating light in the device. This method of measurement would be useful to determine constitutive parameters in such waveguide-based photonic devices, allowing us to design photonic integrated circuits that make use of metamaterials.

OCIS codes: 130.0130, 160.3918, 130.5990.

Optical metamaterials offer new opportunities for innovation in the field of electromagnetic parameter design, such as the design of permittivity ε and permeability μ. The major focus of attention is to create artificial materials with unique ε-μ values that cannot be observed in any existing media and to take advantage of these expanded parameters for better control of electromagnetic waves. Recent progress in optical metamaterials has allowed researchers to move material properties away from the nonmagnetic line $\mu = 1$ and has opened the third quadrant of the parameter space (i.e., $\varepsilon < 0$ and simultaneously $\mu < 0$), which was previously inaccessible [1–5].

Introducing optical metamaterials into actual photonic devices poses an exciting challenge. Much effort has been expended in the development of advanced optical applications using the concept of metamaterials; leading examples of such applications include a fiber-based metamaterial device that can be used as a nanoscale light source [6] and a Si-based metamaterial modulator that can perform negative-index tuning [7–9].

Encouraged by these results, we have started applying optical metamaterials to photonic integrated circuits (PICs) [10] consisting of III-V semiconductor-based waveguide devices. Our objective is the sophisticated manipulation of light signals in PICs, such as wavelength-selective light trapping, negative index modulation, and waveguide cloaking. To move one step closer to this objective, we have developed GaInAsP/InP multimode-interferometers (MMIs) combined with a metamaterial layer consisting of split-ring resonators (SRRs). At a 1.55 μm communication wavelength, non-unity permeability, induced by magnetic interaction between the SRRs and light propagating in the MMI waveguide, was confirmed in the device [11,12]. In waveguide-based photonic devices, it is very important to have an accurate constitutive parameter value (i.e., the complex permittivity and permeability of the SRR-metamaterial layer as a function of frequency), because this factor mainly determines their performance. Accurate permeability data, however, cannot be extracted from the simple transmission data of our previous devices. In this paper, we propose a method of measurement that uses a Mach–Zehnder interferometer (MZI) and is successfully employed to obtain accurate permeability data. Further detail follows.

For the measurement, we prepared two types of devices, as shown in Fig. 1. One is a GaInAsP/InP straight waveguide with a metal SRR array (an SRR-metamaterial layer) on the surface of the waveguide [Fig. 1(a)]. The other is an MZI consisting of two directional couplers and two arms, with an SRR array attached on one of the arms [Fig. 1(b)]. For the TE-mode input light with the SRR-resonance frequency, the SRR array interacts with the propagating light, thereby behaving as a metamaterial layer with non-unity permeability. This affects the transmission characteristics of light, such as the intensity attenuation and phase shift of light traveling in the waveguide. We can measure the intensity attenuation using the straight waveguide and the phase shift using the MZI. From these data, we can derive the effective permeability and permittivity of the SRR array.

We made the devices for use at the 1.5 μm optical communication wavelength, using a GaInAsP epitaxial multilayer on an InP substrate as in our previous devices [8]. On the epitaxial multilayer, SRR arrays (consisting of 10 nm thick Ti and 40 nm thick Au) were formed using electron-beam lithography (EBL) and a lift-off process. Figure 2(a) shows the oblique image of the SRR array observed with a scanning electron microscope (SEM).

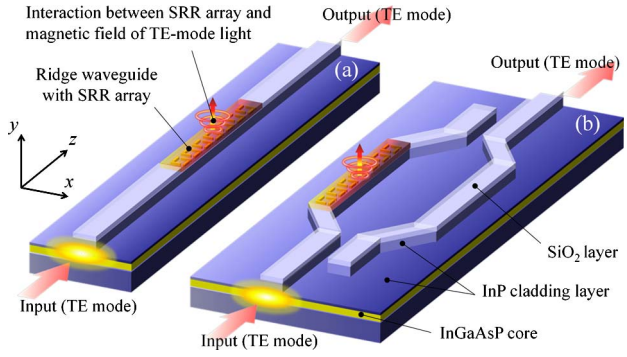

Fig. 1. (Color online) (a) GaInAsP/InP waveguide with SRR array and (b) Mach–Zehnder interferometer consisting of GaInAsP/InP waveguides and SRR array attached on one arm.

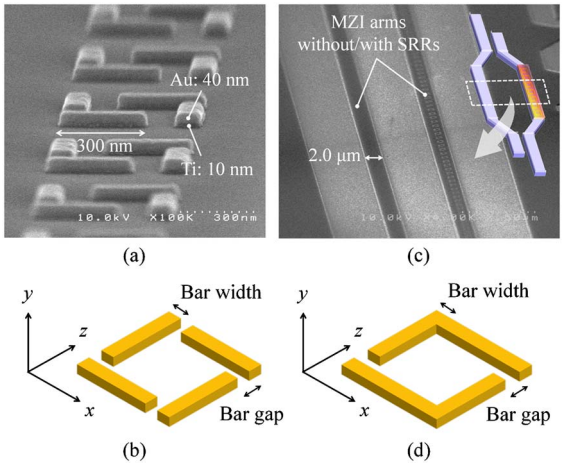

Fig. 2. (Color online) SRRs and arms of MZI: (a) oblique view of four-cut SRRs and (c) two arms, observed with SEM. One arm has an SRR array. Three-dimensional views of (b) four-cut SRR and (d) two-cut SRR.

The *four-cut* SRR shown in Fig. 2(b) was used to obtain resonance at the 1.5 μm band frequency (193 THz), because it has a high resonant frequency owing to its small gap capacitance [13]. The SRR parameters were set as ring size = 300 nm × 300 nm, bar width = 75 nm, bar gap = 75 nm, and array pitch = 585 nm.

After the formation of the SRR array, a SiO_2 mask (100 nm thick) for the MZI (or straight waveguide) pattern was formed on the device with plasma-enhanced chemical vapor deposition and EBL. With the SiO_2 mask, the device structure was formed using CH_4/H_2 reactive ion etching. Figure 2(c) shows the SEM oblique view of the MZI arms with/without the SRR array. The length of the SRR array along the arm was set to 500 μm. In addition to these experimental samples, we prepared control samples with SRRs consisting of *two-cut* square rings [see Fig. 2(d)] with the same size as that of the *four-cut* SRR. The *two-cut* SRR has a resonant frequency of 105 THz, which is lower than 193 THz; therefore, it does not interact with the 1.5 μm light. Table 1 shows the structure and SRR dimension of all the fabricated devices.

In these devices, the electric field E_x (parallel to the x axis shown in Fig. 1) in each layer is given by the scalar wave equation

$$\partial_x^2 E_x + \partial_y^2 E_x + \left(k_0^2 \varepsilon_x \mu_z - \frac{\mu_z}{\mu_y}\beta^2\right) E_x = 0 \qquad (1)$$

for TE-mode light, where ε_x, μ_y, and μ_z are the diagonal elements of the permittivity and permeability tensor, k_0 is the free-space propagation constant, and β is the propagation constant in the device along the z direction.

In the GaInAsP/InP layers, the permeability elements μ_y and μ_z are 1 at optical frequency; therefore, Eq. (1) reduces to the normal wave equations for transverse field components E_x. In contrast, in the SRR array, μ_y shows a non-unity value when the input light has a frequency equal to the SRR resonance frequency (μ_z is constant at 1). Our aim is to determine permittivity $\varepsilon_x = \varepsilon_x' + j\varepsilon_x''$ and permeability $\mu_y = \mu_y' + j\mu_y''$ of the SRR array. There are four unknown parameters ε_x', ε_x'', μ_y', and μ_y'', which can be derived using the measurement devices listed in Table 1. Our method of measurement is as follows.

(I) We first determine the permittivity $\varepsilon_x = \varepsilon_x' + j\varepsilon_x''$ of the *two-cut* SRR array. Permeability μ_y can be set to 1 because *two-cut* SRRs do not interact with the 1.5-μm light. Therefore, we can calculate ε_x from the difference between the transmission characteristics of the device with the *two-cut* SRRs and those of the device without SRRs, measured for the straight waveguides (samples 1 and 2 in Table 1) and MZIs (samples 4 and 5).
(II) The x-direction permittivity ε_x of the SRR array hardly changes for TE-mode light whether or not the SRRs resonate with the light. We confirmed this with electromagnetic simulation based on finite element method. Therefore, the value of ε_x obtained for the *two-cut* SRRs can be used for the *four-cut* SRRs.
(III) Using the ε_x value, we can determine the permeability $\mu_y = \mu_y' + j\mu_y''$ of the *four-cut* SRR array from the difference between the transmission characteristics of the device with *four-cut* SRRs and those of the device with *two-cut* SRRs, measured for the straight waveguides (samples 2 and 3) and MZIs (samples 5 and 6).

Figure 3(a) shows the measured output intensities for the straight waveguides with the *two-cut* SRR array (sample 2), with the *four-cut* SRR array (sample 3), and without the SRR array (sample 1). The four-cut SRRs resonated at approximately 1510–1520 nm and produced maximum loss at this wavelength. The difference between the waveguides without the SRR array and that with the *two-cut* SRR array is shown by the loss caused by light absorption in the SRR metal. The difference between the *two-cut* SRR array and the *four-cut* SRR array corresponds to a loss caused by light absorption in the SRR metal. That is, the difference shows a net loss caused by the magnetic interaction, excluding parasitic elements such as metal absorption loss in the SRRs and lensed-fiber coupling loss in the measurement system.

Table 1. All Parameters Used in the Experiment

Sample No.	Waveguide Structure[a]	SRR Type	Dimensions of Individual SRR	Array Pitch of SRR Cells
1	Straight ridge	None	N/A	N/A
2	Straight ridge	two-cut single	Ring size[b]: 300 × 300 (nm)	585 (nm)
3	Straight ridge	four-cut single	Bar-width: 75 (nm) Bar-gap: 75 (nm)	
4	MZI	None	N/A	N/A
5	MZI	two-cut single	Ring size[b]: 300 × 300 (nm)	585 (nm)
6	MZI	four-cut single	Bar-width: 75 (nm) Bar-gap: 75 (nm)	

[a]Length of SRR array on straight waveguides and MZI arms is 500 μm for all samples.
[b]Inner size of square SRR ring.

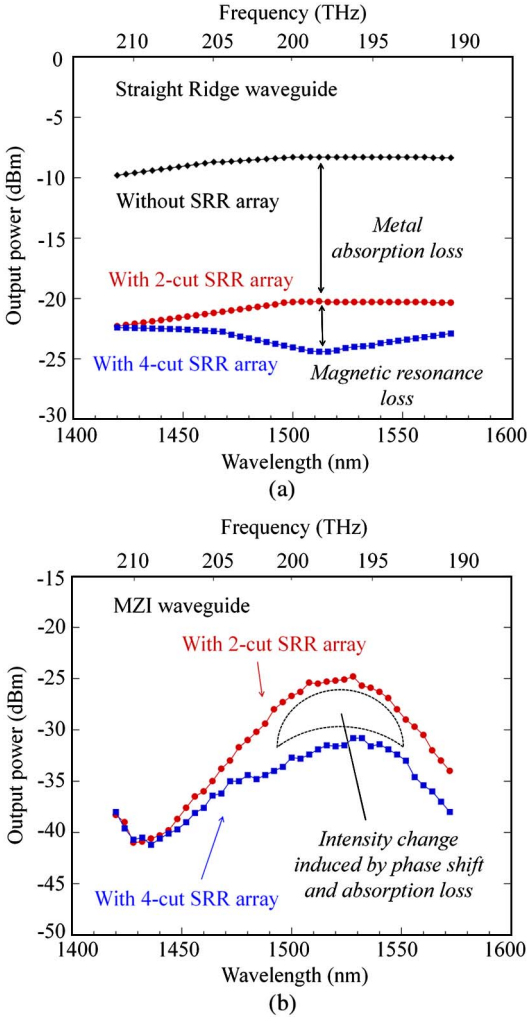

Fig. 3. (Color online) Output intensity in devices with four-cut SRRs (blue lines), two-cut SRRs (red lines), and without SRRs (black lines) as a function of wavelength, measured for (a) straight ridge waveguides and (b) MZIs.

Figure 3(b) shows the output intensities for the MZI with the *two-cut* SRR array (sample 5) and the *four-cut* SRR array (sample 6). Their difference is caused by the phase shift of light induced by the magnetic interaction between the four-cut SRR array and light in the MZI arm. The parasitic elements are excluded, as in the measurement of the straight waveguides.

We prepared additional devices that had larger SRRs, with sizes ranging from 350 to 500 nm^2, and we confirmed that the difference between the *four-cut* SRR array and the *two-cut* SRR array disappeared because a resonant wavelength became longer and exceeded 1.5 μm.

Using the experimental results shown in Fig. 3 and the eigenvalue equations calculated from Eq. (1) based on the finite difference method, we determined the accurate constitutive parameters of the 300×300-nm SRR array layer in the device according to the abovementioned procedure (I)–(III). In this procedure, we assumed that E_x showed an exponential attenuation in the SiO_2: SRR metamaterial layer and the InP substrate. The Dirichlet condition ($E_x = 0$) was used in the air region.

Figure 4 shows the obtained relative permeability (real and imaginary parts) of the SRR array as a function of frequency. The SRRs showed a resonance at 198 THz (1510 nm), and the real part of permeability changed from 2.1 to 0.2 in the vicinity of this frequency. The proposed method of measurement would be useful to determine constitutive parameters in waveguide-based photonic devices combined with metamaterials. With this information, we will be able to design novel PICs that make use of metamaterials.

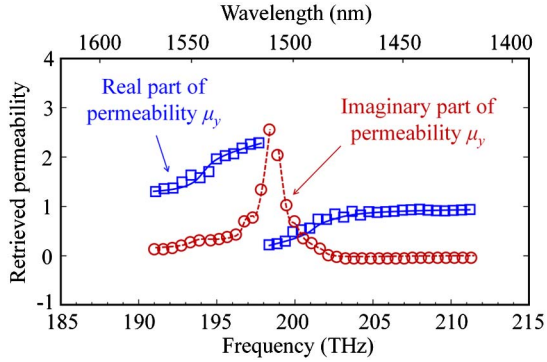

Fig. 4. (Color online) Measured relative permeability (real and imaginary parts) of SRR array on MZI waveguide, plotted as a function of frequency.

This research was financially supported by the Ministry of Education, Culture, Sports, Science and Technology (MEXT), Japan and the Japan Society for the Promotion of Science (JSPS) under Grants-in-Aid for Scientific Research (#19002009, #22360138, #21226010, #23760305, #10J08973).

References

1. S. Linden, C. Enkrich, G. Dolling, M. W. Klein, J. Zhou, T. Koschny, C. M. Soukoulis, S. Burger, F. Schmidt, and M. Wegener, IEEE J. Sel. Topics. Quantum Electron. **12**, 1097 (2006).
2. H. J. Lezec, J. A. Dionne, and H. A. Atwater, Science **316** (5823), 430 (2007).
3. W. Cai, U. K. Chettiar, H. K. Yuan, V. C. de Silva, A. V. Kildishev, V. P. Drachev, and V. M. Shalaev, Opt. Express **15**, 3333 (2007).
4. M. S. Rill, C. E. Kriegler, M. Thiel, G. von Freymann, S. Linden, and M. Wegener, Opt. Lett. **34**, 19 (2009).
5. C. E. Kriegler, M. S. Rill, S. Linden, and M. Wegener, IEEE J. Sel. Topics. Quantum Electron. **16**, 367 (2010).
6. G. Adamo, K. F. MacDonald, F. De Angelis, E. Di Fabrizio, and N. I. Zheludev, in *Proceedings of 23rd Annual Meeting of the IEEE Photonics Society* (2010), paper WM2.
7. K. M. Dani, Z. Ku, P. C. Upadhya, R. P. Prasankumar, S. R. Brueck, and A. J. Taylor, Nano Lett. **37**, 3565 (2009).
8. D. J. Cho, W. Wu, E. Ponizovskaya, P. Chaturvedi, A. M. Bratkovsky, S. Y. Wang, X. Zhang, F. Wang, and Y. R. Shen, Opt. Express **17**, 17652 (2009).
9. K. M. Dani, Z. Ku, P. C. Upadhya, R. P. Prasankumar, A. J. Taylor, and S. R. J. Brueck, Opt. Express **19**, 3973 (2011).
10. L. A. Coldren, S. C. Nicholes, L. Johansson, S. Ristic, R. S. Guzzon, E. J. Norberg, and U. Krishnamachari, J. Lightw. Technol. **29**, 554 (2011).
11. T. Amemiya, T. Shindo, D. Takahashi, N. Nishiyama, and S. Arai, IEEE J. Quantum Electron. **47**, 736 (2011).
12. T. Amemiya, T. Shindo, D. Takahashi, S. Myoga, N. Nishiyama, and S. Arai, Opt. Lett. **36**, 2327 (2011).
13. A. Ishikawa, T. Tanaka, and S. Kawata, J. Opt. Soc. Am. B **24**, 510 (2007).